ACS OMEGA

Open Access

http://pubs.acs.org/journal/acsodf

Article

A-Site Cation Disorder in $Sr_xBa_{1-x}Nb_2O_6$ (x = 0.25, 0.33, 0.50, 0.61) Studied by High-Resolution Resonant X-ray Powder Diffraction

Ola G. Grendal,* Andrew N. Fitch, and Solveig S. Aamlid

Cite This: *ACS Omega* 2023, 8, 37592−37599

Read Online

ACCESS | Metrics & More | Article Recommendations | Supporting Information

ABSTRACT: The dielectric and ferroelectric properties of $Sr_xBa_{1-x}Nb_2O_6$ (SBN, 0.2 < x < 0.8) are known to be affected by the Sr fraction and can be further controlled by various quenching schemes. Changes in A-site cation configuration are believed to be linked to these changes in properties. In this work, we study the A-site cation disorder in SBN by the use of high-resolution resonant X-ray powder diffraction. The experimental results show that the larger Ba^{2+} is found exclusively on the larger A2 site, while Sr^{2+} is found on both the A1 and A2 sites, with an increasing amount on A2 with an increasing Sr fraction. At elevated temperatures, a small migration of Sr^{2+} from A1 to A2 is observed for SBN50 and SBN61. Linking this change in occupancies to changes in the average cation size on the A1 and A2 sites allows for rationalization of the property changes observed for quenched samples. Furthermore, SBN25 is shown to deviate from the tetragonal *P4bm* structure and is found to be orthorhombic with a *Cmm*2 structure.

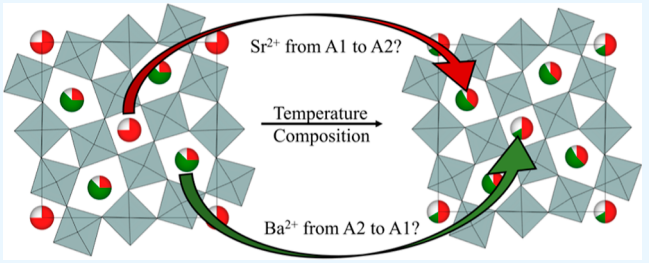

INTRODUCTION

$Sr_xBa_{1-x}Nb_2O_6$ (SBN100x, 0.2 < x < 0.8) is a lead-free ferroelectric material,[1] with good pyroelectric[2,3] and photorefractive properties.[4] SBN is generally found in a tetragonal tungsten bronze (TTB) structure having a general formula of $A1_2A2_4C_4B1_2B2_8O_{30}$ and the polar space group *P4bm* (no. 100) at room temperature;[1,5,6] however, reports exist on orthorhombic distortions for low Sr fractions (x < 0.23).[7] SBN is a so-called unfilled TTB, meaning that the A1 and A2 sites are partially filled by a total of five Sr^{2+} and Ba^{2+} atoms in addition to one vacancy, all free to move between the two sites, which gives a potential for inherent cation disorder in the material. This potential for cation disorder is believed to be responsible for some of the interesting features of this material.

Several studies have reported on how the dielectric and ferroelectric properties of SBN change with different annealing and quenching schemes[8,9] and with composition.[2,10] The cation configuration on the A1 and A2 sites is proposed as a possible explanation.[8,9] Another explanation is the incommensurate tilting patterns of the NbO_6 octahedra that are observed for SBN[11−13] and are a common feature for many TTB materials.[14] These two phenomena could also be correlated.[15] In this work, we are, however, focusing on the cation configuration on the A-sites. The general assumption for the cation configuration is that Sr^{2+} is mainly occupying the smaller A1 site, while Ba^{2+} is mainly occupying the larger A2 site. Additionally, there is a possibility for mixed occupancy on both sites, as reported for the filled TTB, $Ba_4Na_2Nb_{10}O_{30}$ (BNN), having approximately ∼10% of the larger Ba^{2+} going to the smaller A1 site.[16,17] Several works have thus studied the cation configuration in SBN: X-ray powder diffraction,[9,18] combined neutron and X-ray powder diffraction,[5] X-ray single-crystal diffraction,[6,13,19] transmission electron microscopy (TEM),[20] and density functional theory (DFT).[21] However, owing to subtleties in the SBN structure and chemistry, which will be introduced in detail below, it is not clear how these diffraction studies could reliably obtain accurate site occupancies with the exception of the combined neutron and X-ray powder diffraction work. The two cations plus vacancy sharing two sites makes the cation configuration an underdetermined system unless the amount of Ba^{2+} on the A1 site has been assumed to be 0 (or some other assumption that would reduce the complexity), which has often been done.[6,9,13,19,22,23]

By conventional X-ray or neutron diffraction experiments, all site occupancies can typically be obtained by appropriately constraining the refinements in a material with two elements distributed over two atomic sites. Naively, this is the case for SBN since Sr^{2+} and Ba^{2+} are distributed over the A1 and A2 sites, but the high vacancy concentration complicates the analysis. As an example, consider first the case of $Sr_xBa_{1.2-x}Nb_2O_6$ (a vacancy-free, filled version of the normally

Received: August 30, 2023
Accepted: September 14, 2023
Published: September 29, 2023

unfilled SBN).[24] In Table 1, it is shown how the constraints could look for a Rietveld refinement for such a material with

Table 1. Possible Set of Constraints for a Refinement with a Total of 6 Atoms Distributed over Two Atomic Sites for the Filled $Sr_xBa_{1.2-x}Nb_2O_6$[a]

atomic site	cation	occupancy [atoms]
A1	Sr	*SrA1*
A1	Ba	*BaA1* = 1−*SrA1*
A2	Sr	*SrA2* = *TotSr*−*SrA1*
A2	Ba	*BaA2* = *TotBa*−*BaA1*

[a]*SrA1* is the only free parameter, with *TotSr* and *TotBa* being composition-dependent and assumed to be known.

only one free variable (the Sr occupancy on the A1 site, *SrA1*), yielding all 4 site occupancies. This is routinely done and is a typical method for obtaining site occupancies in such cases,[16,17,25] assuming the scattering contrast is sufficiently large between the two atoms in question.

In the case of an unfilled SBN, an extra degree of freedom is introduced with the vacancy that is free to move between the A1 and A2 sites. The effect of this extra variable is that the total occupancy for neither site can be determined anymore. Table 2

Table 2. Possible Set of Constraints for a Refinement with a Total of 5 Atoms and 1 Vacancy Distributed over Two Atomic Sites for the Unfilled $Sr_xBa_{1-x}Nb_2O_6$[a]

atomic site	cation	occupancy [atoms]
A1	Sr	*SrA1*
A1	Ba	*BaA1* = *Tot_occA1*−*SrA1*
A2	Sr	*SrA2* = *TotSr*−*SrA1*
A2	Ba	*BaA2* = *TotBa*−*BaA1*

[a]*Tot_occA1* and *SrA1* are the two free parameters. *TotSr* and *TotBa* are composition-dependent and assumed to be known.

shows how such refinement could be constrained by introducing one new free parameter to the refinement, namely, the total occupancy on the A1 site (*Tot_occA1*). This gives two free variables, i.e., *Tot_occA1* and *SrA1*.

For a conventional diffraction experiment, these two free parameters are 100% correlated in the case of the unfilled SBN. The reason for this is the combination of the extra degree of freedom imposed by the vacancy and the fact that the shapes of the atomic form factors are almost identical for Sr^{2+} and Ba^{2+}, except for a scaling factor. This last point is highlighted in Figure 1a, where the ratios between the two atomic form factors are plotted. In the absence of any significant resonant contribution, the ratio is close to constant over a wide range in Q. This in combination with the extra degree of freedom from the vacancy yields a range of equally plausible cation configurations (synthesized in Figure 1b). Essentially, it is impossible to tell the scattering strength of 1.5 × Sr^{2+} + 0.5 × vacancy from 1 × Ba^{2+} + 1 × vacancy (configurations 1 and 2 in Figure 1b).

The ratio between the two atomic form factors can be affected by performing resonant (also called anomalous) X-ray diffraction (XRD).[26] This is typically done to increase the scattering contrast between similar elements,[27,28] but it can also be used to change the shape of an element's atomic form factor, as shown in Figure 1a. In the case of SBN, we argue that this provides enough information to reduce the parameter

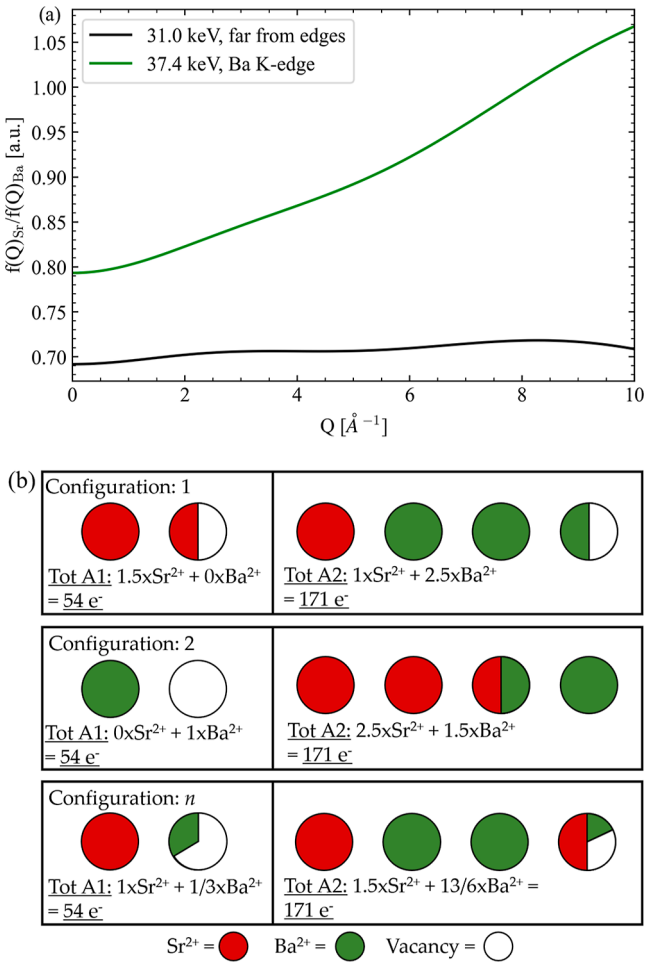

Figure 1. (a) Ratio between the atomic form factors for Sr^{2+} and Ba^{2+} ($f(Q) = f_0(Q) + f'$, where $f_0(Q)$ is the coherent scattering factor, f' is the real part of the anomalous dispersion correction, Q is the scattering vector, and the imaginary part of the anomalous dispersion correction f'' is omitted for simplicity) at two energies up to 10 $Å^{-1}$. More energies are presented in Figure S1. (b) Three hypothetical cation configurations for $Sr_{0.5}Ba_{0.5}Nb_2O_6$, all identical from a refinement point of view when only considering the total number of electrons on each site.

correlation, and thus all 4 site occupancies can be obtained when performing a combined Rietveld refinement of data collected at several energies, of which at least one is close to an absorption edge of either Sr or Ba. It is worth mentioning that this issue will also be the case for neutron diffraction, in fact, even more so as the neutron scattering length is constant as a function of Q. However, combining neutrons and XRD is analogous to combining X-ray resonant scattering and conventional XRD. Although X-ray resonant scattering is less accessible than conventional XRD and requires access to an X-ray beam with tunable energy, it is preferred over neutron diffraction, which requires a larger sample volume and longer counting times and has fewer facilities worldwide. Additionally, X-ray resonant scattering avoids any ambiguities that can arise from performing one X-ray and one neutron diffraction experiment (i.e., different temperatures, sample volumes, and even samples).

As is clear from the discussion above, in the case of unfilled SBN (a vacancy giving an extra degree of freedom and the very similar shape of the atomic form factors of the atoms in

https://doi.org/10.1021/acsomega.3c06500
ACS Omega 2023, 8, 37592−37599

question), a single neutron or XRD experiment cannot be used to determine all 4 site occupancies due to strong parameter correlations. This could be the cause of the "aberrant results" reported in previous works attempting to extract all 4 site occupancies from a single X-ray powder diffraction pattern.[18] However, X-ray resonant scattering can be used to gain extra information to reduce this correlation, not in the conventional way of increasing the scattering contrast but by significantly changing the shape of the atomic form factors of either Sr^{2+} or Ba^{2+} in this case.

In this work, we use high-resolution resonant X-ray scattering to study the cation configurations of SBN25, SBN33, SBN50, and SBN61, extending the work of Carrio et al.[5] to the Ba-rich part of the SBN phase diagram. The cation configuration is also studied as a function of temperature at room temperature (RT), 300, 800, and 1000 °C. The results are discussed with respect to existing literature on the dielectric and ferroelectric properties of SBN as a function of the Sr fraction and quenching schemes. Furthermore, SBN25 is shown to deviate from the accepted tetragonal symmetry and is found to be orthorhombic.

MATERIALS AND METHODS

SBN with four compositions, $Sr_{0.25}Ba_{0.75}Nb_2O_6$ (SBN25), $Sr_{0.33}Ba_{0.67}Nb_2O_6$ (SBN33), $Sr_{0.50}Ba_{0.50}Nb_2O_6$ (SBN50), and $Sr_{0.61}Ba_{0.39}Nb_2O_6$ (SBN61), were prepared by solid-state synthesis as described in more detail previously.[9] Powders were obtained by gently grinding the as-obtained pellets. The powders were contained in 0.5 mm glass capillaries. High-resolution resonant XRD data were collected in transmission geometry on the high-resolution setup at the ID22 beamline, European Synchrotron Radiation Facility (ESRF), Grenoble, France.[29] The position of the Ba K-edge was obtained by measuring the X-ray fluorescence for SBN25 and SBN61 while scanning the energy across the Ba K-edge (37.2−37.6 keV). From this, 3 different energies, 31 keV (far away from Ba K-edge, λ = 0.39984 Å), 37.433 keV (pre Ba K-edge, λ = 0.33121 Å), and 37.448 keV (inflection point Ba K-edge, λ = 0.33109 Å), were selected for the diffraction experiments, and powder diffraction patterns were collected up to a Q of around 10 $Å^{-1}$. A silicon standard (NIST, 640c) was used to calibrate the energies. A hot-air blower was used to control the temperature at 300, 800, and 1000 °C.

For each composition, the three datasets were refined together in a combined Rietveld refinement using TOPAS (version 7).[30] The dispersion corrections f' and f'' for Ba^{2+} were obtained from the X-ray fluorescence data using *kkcalc*,[31] see Figure S2 in the Supporting Information. Based on the almost perfectly overlapping f' and f'' curves, it was decided to use the average of these to obtain the anomalous dispersion corrections for the Rietveld refinement for all compositions. The remaining dispersion corrections (Sr^{2+}, Nb^{5+}, and O^{2-} at all 3 energies and Ba^{2+} at 31 keV) were taken from the tables of Sasaki.[32] All f' and f'' used are presented in Table 3. Note that implicit in this analysis is the fact that the Nb and O atom positions are fully occupied and thus act as an overall scaling of the data.

All room temperature patterns were modeled in space group *P4bm* and the high temperature patterns in *P4/mbm*. The SBN25 room temperature data was modeled in *Cmm2*. For all refinements, a set of lattice parameters (needed because of beam heating), zero error, and scale factor were refined individually for each energy. The background was modeled with straight line segments between manually set points selected individually for each diffraction pattern, with a corresponding overall scale factor for the manually selected points. Combined for all energies, a *Simple_Axial_Model* asymmetry parameter, Gaussian and Lorentzian strain broadening parameters, five thermal parameters (one for each Nb-site, one for A1, one for A2, and one for all oxygen sites), atomic site parameters (11 for *P4/mbm*, 18 for *P4bm*, and 33 for *Cmm2*), and two occupancy mixing parameters for the A1 and A2 sites were refined. For *P4bm* and *P4/mbm*, refining the A2 site as a split site with half occupancy was observed to improve the refinements significantly (i.e., moving the atom away from a mirror plane). This gives a total of 36, 43, and 58 free parameters for *P4/mbm*, *P4bm*, and *Cmm2*, respectively. The constraints and limits used for the occupancy parameters are listed in Table 4. Alternative approaches were tested (e.g., using *BaA1* as a free parameter and constraining *SrA1*) and yielded identical results.

Table 3. Dispersion Corrections, f' and f'' (f'/f'') Used for the Rietveld Refinements

atom	31 keV	37.433 keV	37.448 keV
Ba^{2+}	−1.771/0.818	−6.976/1.338	−7.529/2.765
Sr^{2+}	0.128/1.234	0.135/0.872	0.135/0.872
Nb^{5+}	−0.011/1.624	0.077/1.159	0.077/1.159
O^{2-}	−0.002/0.002	−0.004/0.001	−0.004/0.001

Table 4. Constraints and Limits Used for the Refined A1 and A2 Site Occupancy Mixing Parameters[a]

atomic site	cation	parameter name	constraint	limits (min/max)
A1	N/A	*Tot_occA1*	Free	0.5/1
A1	Sr	*SrA1*	Free	0/*Tot_occA1*[b]
A1	Ba	*BaA1*	=*Tot_occA1*−*SrA1*	N/A
A2	Sr	*SrA2*	=*TotSr*−*SrA1*	N/A
A2	Ba	*BaA2*	=*TotBa*−*BaA1*	N/A

[a]*TotSr* and *TotBa* are composition-dependent and assumed to be known. [b]It was made sure that *SrA1* could not be higher than the total amount of Sr for a given composition, but in practice, *SrA1* was always limited by *Tot_occA1*.

In the absence of access to resonant diffraction techniques, the bond valence sum (BVS) method has been used to identify the relative occupancy and oxidation states in solid solutions.[33] In this technique, cation−anion bond lengths and coordination numbers are compared with tabulated values. *VaList*[34] and the tabulated values from Brown and Altermatt[35] were used to calculate BVS from the refined room temperature structures in this work.

RESULTS

All samples studied were phase pure within the detection limit of XRD and the diffraction patterns showed no deviation from the accepted average *P4bm* structure, with the exception of SBN25. At elevated temperatures, all samples matched with the *P4/mbm* structure, and no satellite reflections were observed for any samples. A representative Rietveld refinement of SBN33 at room temperature is presented in Figure 2, showing the 31 and 37.446 keV diffraction patterns. The inset shows the low-Q region, where the most notable effect of the on/off-edge measurements is observed as small changes in the

https://doi.org/10.1021/acsomega.3c06500
ACS Omega 2023, 8, 37592−37599

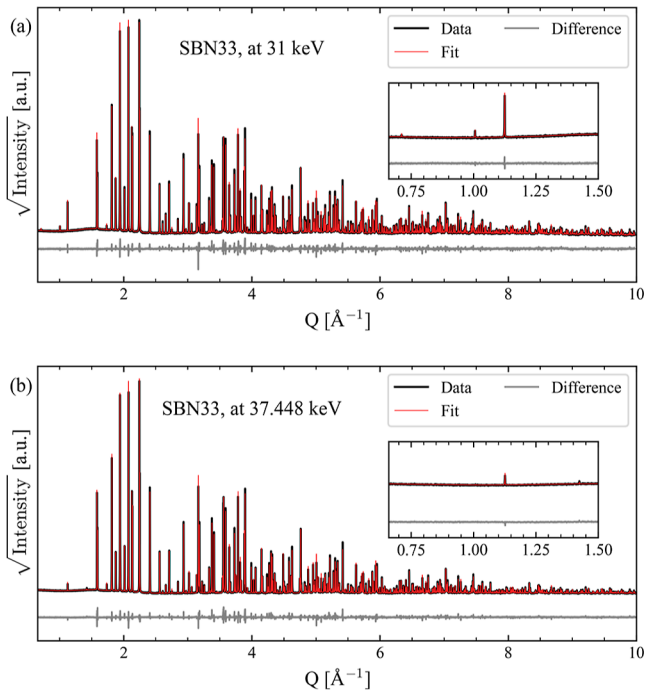

Figure 2. Representative Rietveld refinement of the (a) 31 and (b) 37.448 keV XRD patterns of SBN33 collected at room temperature. The inset shows the low-*Q* region where the most notable effect of being close to the Ba K-edge is observed, highlighting how these subtle differences are well fitted. R_{exp} = 1.31%, R_{wp} = 6.53%, and GOF = 5.00.

relative intensities of the reflections. Refined structural parameters for all compositions at room temperature are presented in Tables S1−S4 in the Supporting Information.

A-Site Cation Configuration. For all compositions, the occupancy of Ba^{2+} on the A1 site (*BaA1*) refined to 0, see Figure 3a. Although previous studies have typically assumed this to be the case, we believe this is the first time this is actually reliably confirmed by Rietveld refinement, giving solid support to previously reported values. It has to be mentioned that the fact that the value is exactly equal to 0 is because the occupancy of Sr^{2+} on A1 (*SrA1*) is always refined to its maximal value (see Table 1), thus constraining *BaA1* to be 0. Removing the upper limit on *SrA1* resulted in unphysical negative values for *BaA1*, typically in the range ∼−0.05(1), and insignificant improvements on the overall fit. Based on this and considering the uncertainties of obtaining site occupancies from X-ray powder diffraction data, it seems clear that the A1 site is occupied solely by Sr^{2+} in SBN. This strong preference for the Ba^{2+} to occupy only the larger A2 site is also supported by the BVS analysis. The BVS for Ba^{2+} is close to the ideal value of 2+ on the A2 site for all compositions, while it is significantly overbonded on the smaller A1 site, as shown in Figure 3b. Similarly, the BVS of Sr^{2+} on the A1 site is close to the ideal value, while it is underbonded on the larger A2 site. Note that SBN25 (owing to the orthorhombic symmetry) has two symmetrically distinct and slightly differently sized A2 sites and hence the two data points.

With increasing Sr fractions, the most striking feature is the close to near-linear increase in Sr^{2+} on A2 (*SrA2*) and the corresponding decrease in Ba^{2+} on A2 (*BaA2*), as shown in Figure 3a. Only relatively small changes are observed for Sr^{2+} on A1 (*SrA1*) and the total occupancy on the A1 and A2 sites

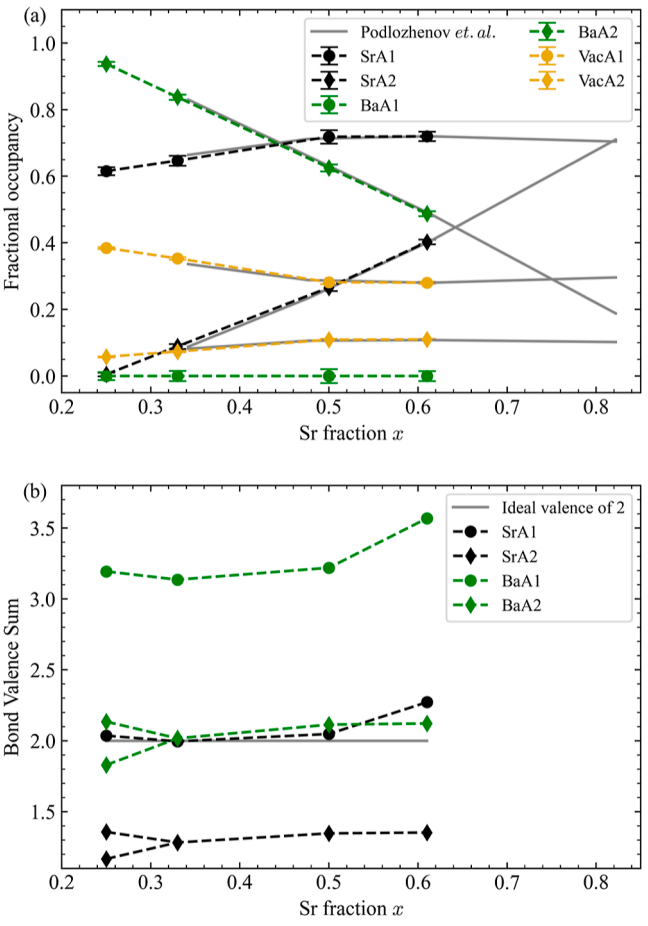

Figure 3. (a) Fractional site occupancies for the A1 and A2 sites in SBN at room temperature as a function of Sr fraction *x*. Gray lines are taken from Podlozhenov et al.[6] and show excellent agreement with this work. Error bars show the standard uncertainties (esds) as obtained from the Rietveld refinements. (b) BVS for Ba^{2+} and Sr^{2+} on both the A1 and A2 sites from the refined room temperature structures. The gray line shows an ideal valence of 2+. Note that SBN25 (owing to the orthorhombic symmetry) has two symmetrically distinct and slightly differently sized A2 sites and hence the two data points.

(presented as the vacancy occupancy in Figure 3a, with *VacA1* = 1 − *SrA1* − *BaA1* and *VacA2* = 1 − *SrA2* − *BaA2*) as a function of Sr fraction. The values obtained in this work are in excellent agreement with the work of Podlozhenov et al.[6] and Carrio et al.[5] and the general trends in other studies.[9,13]

Knowing that there is a significant parameter correlation between the two free occupancy parameters (*SrA1* and *Tot_occA1*), several refinements were performed with *SrA1* fixed at various values, covering physically plausible values, and recording the R_{wp} as a measure of the quality of the fit. The results are presented in Figure 4. There is a minimum for the obtained R_{wp} values plotted against the *SrA1* values, although the minimum is shallow, especially for SBN25 (see Figure S3 for a better visualization of this for SBN25). Importantly, the minimum corresponds very well with the values obtained from the Rietveld refinements where *SrA1* is not fixed, indicating that the site occupancy fractions presented in this work are at least close to representing the real cation configurations of the studied samples.

Cation Configuration Temperature Dependence. Figure 5 shows the temperature dependence of selected

https://doi.org/10.1021/acsomega.3c06500
ACS Omega 2023, 8, 37592−37599

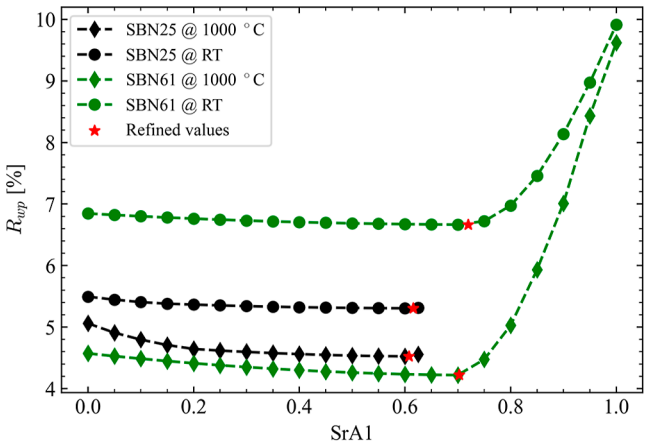

Figure 4. R_{wp} was obtained by Rietveld refinement for a selection of fixed *SrA1* values for various samples and temperatures studied in this work. The red stars mark the values obtained when *SrA1* was refined and not fixed.

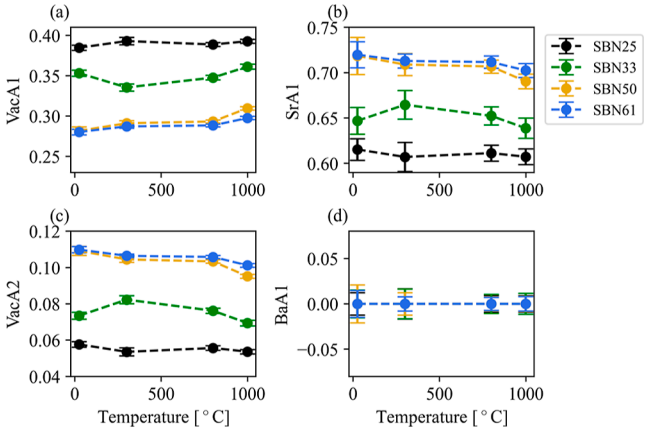

Figure 5. Fractional site occupancies as a function of temperature for SBN25, SBN33, SBN50, and SBN61 show the (a) vacancy (*VacA1*), (b) Sr^{2+} (*SrA1*), and (d) Ba^{2+} (*BaA1*) fractions on the A1 site, and the vacancy fraction (c) (*VacA2*) on the A2 site. Error bars show the estimated standard deviations (esds) as obtained from the Rietveld refinements.

fractional site occupancies for all of the samples studied in the high-temperature experiments. *BaA1* is 0 for all samples at all temperatures and is always constrained to 0 because *SrA1* refines to its maximal value, as explained above. For SBN25, there seems to be no change as a function of temperature within the estimated standard deviations (esds). For SBN50 and SBN61, a small but significant increase in *VacA1* is observed, especially for the highest temperature. Knowing that *BaA1* is always 0 suggests a migration of Sr^{2+} from the A1 site to the A2 site with increasing temperature. This is also confirmed by decreases in *SrA1* and *VacA2* for the same samples at the same temperatures. For SBN33, there might be a small migration of Sr^{2+} from the A1 to the A2 site, as for SBN50 and SBN61, but the trend is less conclusive.

Room-Temperature Structure of SBN25. As opposed to the other compositions studied in this work, SBN25 shows clear deviations from the accepted average tetragonal *P4bm* structure at room temperature, observed most clearly as peak splitting of the (*hk*0) reflections at higher *Q*. This leads to unsatisfactory fits to the data with the *P4bm* structure, as shown in Figure 6a, and suggests symmetry lowering from a

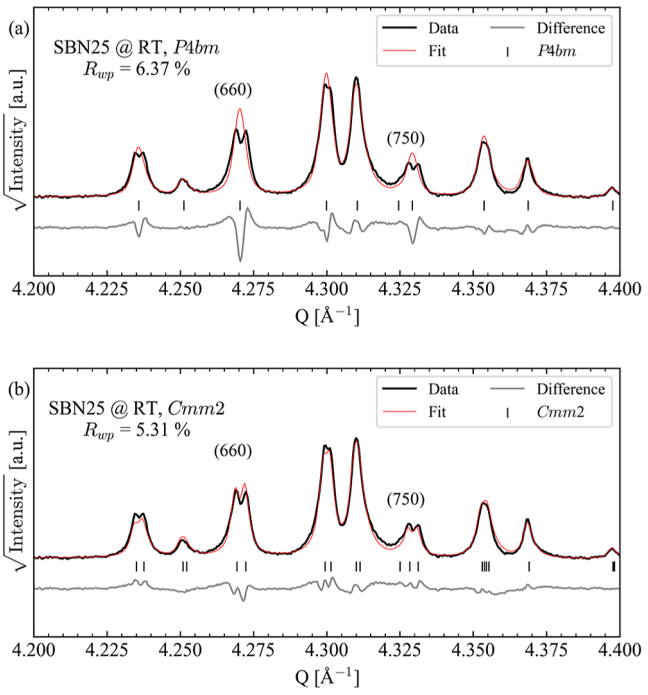

Figure 6. Selected regions of the Rietveld refinement of SBN25 using the (a) *P4bm* and (b) *Cmm*2 structures, show that SBN25 at room temperature is orthorhombic and not tetragonal, as previously reported.[1]

tetragonal to an orthorhombic symmetry. The *Cmm*2 space group is an orthorhombic subgroup of *P4bm* (with a $2^{1/2} \times 2^{1/2} \times 1$ unit cell relative to *P4bm*) and has been proposed for other TTBs.[36] Fitting the SBN25 data with a *Cmm*2 structure transformed from *P4bm* gives an excellent fit to the data, see Figure 6b. The refined lattice parameters are a = 17.66237(4), b = 17.67483(4), and c = 3.983238(8). The refined structural parameters of SBN25 are presented in Table S1.

DISCUSSION

A-Site Cation Configuration. The extra degree of freedom caused by the vacancy present in the unfilled SBN structure has made it challenging to obtain all 4 A-site occupancies reliably, and the typical assumption to avoid this has been that the larger Ba^{2+} (ionic radii 1.61 Å in a XII-coordinated environment[37]) is only occupying the larger A2 site, while Sr^{2+} (ionic radii 1.44 in a XII-coordinated environment Å[37]) has been free to occupy both the A1 and A2 sites. The results in this work clearly show that this assumption is accurate.

This is in contrast to what is observed for the filled BNN structure, where ∼10% Ba^{2+} is found on the A1 site,[16,17] although with larger differences in ionic radii between Na^{+} (ionic radius 1.2 Å[37]) and Ba^{2+} in BNN compared with Sr^{2+} and Ba^{2+} in SBN. The BVS was also calculated for BNN, BKN ($Ba_4K_2Nb_{10}O_{30}$), and BRbN ($Ba_4Rb_2Nb_{10}O_{30}$), all filled TTBs reported elsewhere.[17] These compounds allow the occupation to be determined by a single XRD experiment, and it is known that substantial amounts of Ba go to the A1 site, especially in the case of BKN and BRbN. Interestingly, the BVS for Ba on the A1 site is in the same range as for SBN (3.48, 3.10, and 2.97 for BNN, BKN, and BRbN, respectively). This indicates that it is not impossible for Ba to go to A1 in SBN from a size perspective but that the other elements that are present make a

https://doi.org/10.1021/acsomega.3c06500
ACS Omega 2023, 8, 37592−37599

significant difference. This highlights the limitations of the BVS technique in the case of TTBs, and it explains why resonant diffraction (or neutron diffraction) is the only way to obtain a reliable measure of the site occupancies in these materials once there are more than two species present.

It is reasonable to assume that the same competition between entropy promoting mixed occupancy and more disorder and order driven by the relative ionic radii of the cations and the A1 and A2 sites are present for both SBN and BNN (and all other TTBs). It also seems reasonable that the difference between SBN and BNN could then be explained based on the main difference between them, namely, the vacancy in SBN. The vacancy enables there to be mixed occupancy on only one site (the A2 site in the case of SBN), effectively allowing Sr^{2+} to move from A1 to A2 without having to move Ba^{2+} the other way. In the case of BNN, any movement of Ba^{2+} from A2 to A1 would have to be accompanied by an equal amount of Na^{+} moving the other way, resulting in some Ba^{2+} being blocked on the smaller and less preferred A1 site. SBN has a vacancy concentration orders of magnitude higher than BNN, leading to faster diffusion enabling SBN to exhibit a preferred cation configuration based on cation/site size constraints, resulting in all of the Ba^{2+} being found on the preferred larger site. Relatively small changes as a function of temperature are observed, and the most notable changes are seen for SBN50 and SBN61 at the highest temperature, where ∼2% Sr^{2+} migrates from the smaller A1 to the larger A2 site relative to the room temperature configuration. This is consistent with quenching studies by Graetsch,[19] where only quenching from above 700 °C resulted in Sr^{2+} moving from the A1 to the A2 site for SBN52. Quenching from lower temperatures did not yield any significant changes in the cation configuration. It cannot be ruled out that more cation movement and even the migration of Ba^{2+} to the A1 site can occur at higher temperatures than was studied here.

Considering only the average cation size on A1 and A2 (defined as the sum of the site occupancies multiplied by the respective ionic radii), moving Sr^{2+} from A1 to A2 results in an increase in the average cation size of A2 and a decrease for A1. This can be viewed as analogous to decreasing the Sr fraction, and one could expect that the properties of quenched samples (assuming an increased Sr/Ba ratio on the A2 site can be frozen in) would move toward the properties of SBN with a lower Sr fraction. Such an assessment is in good agreement with the literature. For example, the Curie temperature for SBN decreases with increasing Sr fraction, and Aamlid et al.[9] observed an increasing Curie temperature for quenched SBN, i.e., properties moving toward properties of lower Sr fraction. Furthermore, SBN is known to become more relaxor-like with increasing Sr fractions, and Guo et al.[8] reported that quenched SBN75, SBN60, and SBN50 become less relaxor-like (i.e., a narrowing of the dielectric permittivity peak across the ferroelectric phase transition) and an increase in Curie temperature in accordance with Aamlid et al.

As a final note, whenever a model used for Rietveld refinement hits some physical limits, as the *BaA1* parameter does in our refinement, some critical evaluation is necessary. We hypothesize that imperfections in our model could be uncertainties around the true composition (taken to be the nominal composition from synthesis in this work) or Schottky defects (oxygen-cation vacancy pairs). Both of these could be assumed to affect the relative intensities in the diffraction pattern but are outside the scope of the presented dataset. However, the fact that *BaA1* only barely goes negative when allowed and the overall quality of the Rietveld refinement would suggest that the true values for either of these two (or other effects not considered) are not far from the assumptions used in this work.

Room-Temperature Structure of SBN25. The average room-temperature structure of SBN has generally been accepted to be the polar *P4bm* structure since it was first solved by Jamieson et al.[1] and has been subject to much less discussion around its structure than other TTBs.[38] However, with improved instrumentation and structural characterization techniques, several studies have reported deviations from tetragonal symmetry, both for the average structure for low Sr fractions ($x < 0.23$)[7] and the incommensurate structure at high Sr fractions ($x > 0.82$).[13] This work adds to this, showing that the average structure of SBN25 is orthorhombic, with space group *Cmm*2, thus pushing the transition from orthorhombic to tetragonal to higher Sr fractions than previously reported. The *Cmm*2 space group has the potential to be ferroelastic, and it is not known whether the ferroelectric and ferroelastic transitions coincide in this material.

CONCLUSIONS

Resonant high-resolution XRD data have been used to study the A-site cation configurations in SBN as a function of both the Sr fraction and temperature. The use of resonant X-ray powder diffraction has for the first time allowed the accurate experimental determination of all 4 site occupancy parameters and shows a strong preference for the larger Ba^{2+} cation toward the larger A2 site, with no Ba^{2+} found on the A1 site. This gives an important supplement and credibility to the existing literature. With increasing Sr fractions, there is a close to linear increase of Sr^{2+} on the A2 site, with only small changes in Sr^{2+} on the A1 site. For the high-temperature experiments, the largest effect is observed for SBN61 at the highest temperature, where ∼2% of Sr^{2+} moves from A1 to A2, while Ba^{2+} stays at the A2 site for all samples and for all temperatures. Linking these changes in occupancy as a function of temperature to changes in average cation size on both sites shows that the changing cation configuration is analogous to a decrease in the overall Sr fraction. This is also supported by the changes in properties observed in quenched samples, where their properties evolve toward those of a sample with a lower Sr fraction.

Additionally, SBN25 was proven to deviate from the generally accepted tetragonal *P4bm* space group and was found to be better described by the orthorhombic *Cmm*2 space group.

ASSOCIATED CONTENT

Supporting Information

The Supporting Information is available free of charge at https://pubs.acs.org/doi/10.1021/acsomega.3c06500.

Atomic form factors of Sr^{2+} and Ba^{2+} at additional energies, measured X-ray fluorescence, R_{wp} as a function of *SrA1* for SBN25, and refined structural parameters (PDF)

https://doi.org/10.1021/acsomega.3c06500
ACS Omega 2023, 8, 37592−37599

AUTHOR INFORMATION

Corresponding Author

Ola G. Grendal − *European Synchrotron Radiation Facility (ESRF), 38000 Grenoble, France;* Present Address: Department of Materials Science and Engineering, NTNU Norwegian University of Science and Technology, Trondheim 7491, Norway; orcid.org/0000-0002-4589-8737; Email: ola.g.grendal@ntnu.no

Authors

Andrew N. Fitch − *European Synchrotron Radiation Facility (ESRF), 38000 Grenoble, France*

Solveig S. Aamlid − *Stewart Blusson Quantum Matter Institute, The University of British Columbia, V6T 1Z4 Vancouver, British Columbia, Canada*

Complete contact information is available at: https://pubs.acs.org/10.1021/acsomega.3c06500

Author Contributions

S.S.A. and O.G.G. conceived and planned the work. S.S.A. made the samples. O.G.G. and A.N.F. conducted the data collection. O.G.G. did the data analysis and wrote the first manuscript. All authors discussed the data analysis and interpretation of the data and gave contributions to the final manuscript. All authors have given their approval to the final version of the manuscript.

Notes

The authors declare no competing financial interest.

ACKNOWLEDGMENTS

The European Synchrotron Radiation Facility (ESRF) is greatly acknowledged for giving beam time at ID22 (proposal no. hc4783). The authors thank Dr. Donald Evans for valuable discussion.

ABBREVIATIONS

SBN, strontium barium niobate; TTB, tetragonal tungsten bronze; BNN, barium sodium niobate; TEM, transmission electron microscopy; DFT, density functional theory; XRD, X-ray diffraction; BVS, bond valence sum; BKN, barium potassium niobate; BRbN, barium rubidium niobate

REFERENCES

(1) Jamieson, P. B.; Abrahams, S. C.; Bernstein, J. L. Ferroelectric Tungsten Bronze-type Crystal Structures. I. Barium Strontium Niobate $Ba_{0.27}Sr_{0.75}Nb_2O_{5.78}$. *J. Chem. Phys.* **1968**, *48* (11), 5048−5057.

(2) Glass, A. M. Investigation of the Electrical Properties of $Sr_{1-x}Ba_xNb_2O_6$ with Special Reference to Pyroelectric Detection. *J. Appl. Phys.* **1969**, *40* (12), 4699−4713.

(3) Tang, H.; Tang, X.-G.; Li, M.-D.; Liu, Q.-X.; Jiang, Y.-P. Pyroelectric Energy Harvesting Capabilities and Electrocaloric Effect in Lead-Free $Sr_xBa_{1-x}Nb_2O_6$ Ferroelectric Ceramics. *J. Alloys Compd.* **2019**, *791*, 1038−1045.

(4) Ewbank, M. D.; Neurgaonkar, R. R.; Cory, W. K.; Feinberg, J. Photorefractive Properties of Strontium-barium Niobate. *J. Appl. Phys.* **1987**, *62* (2), 374−380.

(5) Carrio, J. G.; Mascarenhas, Y. P.; Yelon, W.; Santos, I. A.; Garcia, D.; Eiras, J. A. Structure Refinement of (Sr,Ba) Nb_2O_6 Ceramic Powder from Neutron and X-Rays Diffraction Data. *Mater. Res.* **2002**, *5*, 57−62.

(6) Podlozhenov, S.; Graetsch, H. A.; Schneider, J.; Ulex, M.; Wohlecke, M.; Betzler, K. Structure of Strontium Barium Niobate $Sr_xBa_{1-x}Nb_2O_6$ (SBN) in the Composition Range $0.32 < x < 0.82$. *Acta Crystallogr., Sect. B: Struct. Sci., Cryst. Eng. Mater.* **2006**, *62* (6), 960−965.

(7) Nishiwaki, S.; Takahashi, J.; Kodaira, K.; Kishi, M. Morphotropic Phase Boundry and Dielectric Properties of V_2O_5-Containing $Sr_xBa_{1-x}Nb_2O_6$ ($0.2 < x < 0.4$) Ferroelectrics. *Jpn. J. Appl. Phys.* **1996**, *35*, 5137−5140.

(8) Guo, R.; Bhalla, A. S.; Burns, G.; Dacol, F. H. Studies on Annealing and Quenching of Strontium Barium Niobate (SBN) Single Crystals: A-Site Cation Ordering-Disordering Effect. *Ferroelectrics* **1989**, *93* (1), 397−405.

(9) Aamlid, S. S.; Selbach, S. M.; Grande, T. The Effect of Cation Disorder on Ferroelectric Properties of $Sr_xBa_{1-x}Nb_2O_6$ Tungsten Bronzes. *Materials* **2019**, *12* (7), 1156.

(10) Zhang, J.; Wang, G.; Gao, F.; Mao, C.; Cao, F.; Dong, X. Influence of Sr/Ba Ratio on the Dielectric, Ferroelectric and Pyroelectric Properties of Strontium Barium Niobate Ceramics. *Ceram. Int.* **2013**, *39* (2), 1971−1976.

(11) Bursill, L. A.; Lin, P. J. Incommensurate Superstructures and Phase Transition of Strontium Barium Niobate (SBN). *Acta Crystallogr., Sect. B: Struct. Sci., Cryst. Eng. Mater.* **1987**, *43* (1), 49−56.

(12) Woike, T.; Petricek, V.; Dusek, M.; Hansen, N. K.; Fertey, P.; Lecomte, C.; Arakcheeva, A.; Chapuis, G.; Imlau, M.; Pankrath, R. The Modulated Structure of $Ba_{0.39}Sr_{0.61}Nb_2O_6$. I. Harmonic Solution. *Acta Crystallogr., Sect. B: Struct. Sci., Cryst. Eng. Mater.* **2003**, *59* (1), 28−35.

(13) Graetsch, H. A. Large Structural Modulations in the Relaxor Ferroelectric and Intermediate State of Strontium Rich Members ($X > 0.6$) of the $Sr_xBa_{1-x}Nb_2O_6$ (Sbn) Solid Solution Series. *J. Solid State Chem.* **2017**, *246*, 167−175.

(14) Zhu, X.; Fu, M.; Stennett, M. C.; Vilarinho, P. M.; Levin, I.; Randall, C. A.; Gardner, J.; Morrison, F. D.; Reaney, I. M. A Crystal-Chemical Framework for Relaxor versus Normal Ferroelectric Behavior in Tetragonal Tungsten Bronzes. *Chem. Mater.* **2015**, *27* (9), 3250−3261.

(15) Schefer, J.; Schaniel, D.; Petříček, V.; Woike, T.; Cousson, A.; Wöhlecke, M. Reducing the Positional Modulation of NbO_6-Octahedra in $Sr_xBa_{1-x}Nb_2O_6$ by Increasing the Barium Content: A Single Crystal Neutron Diffraction Study at Ambient Temperature for x = 0.61 and x = 0.34. *Z. fur Krist.—Cryst. Mater.* **2008**, *223* (6), 399−426.

(16) Aamlid, S. S.; Selbach, S. M.; Grande, T. Structural Evolution of Ferroelectric and Ferroelastic Barium Sodium Niobate Tungsten Bronze. *Inorg. Chem.* **2020**, *59* (12), 8514−8521.

(17) Nylund, I. E.; Løndal, N. S.; Walker, J.; Vullum, P. E.; Einarsrud, M. A.; Grande, T. Cation Disorder in Ferroelectric $Ba_4M_2Nb_{10}O_{30}$(M = Na, K, and Rb) Tetragonal Tungsten Bronzes. *Inorg. Chem.* **2022**, *61* (39), 15540−15546.

(18) Trubelja, M. P.; Ryba, E.; Smith, D. K. A Study of Positional Disorder in Strontium Barium Niobate. *J. Mater. Sci.* **1996**, *31* (6), 1435−1443.

(19) Graetsch, H. A. Structural Changes of Relaxor Ferroelectric $Sr_{0.52}Ba_{0.48}Nb_2O_6$ (SBN52) on Quenching and Reheating. *Acta Crystallogr., Sect. B: Struct. Sci., Cryst. Eng. Mater.* **2017**, *73*, 820−826.

(20) López-Conesa, L.; Rebled, J. M.; Ruiz-Caridad, A.; Torres-Pardo, A.; Ruiz-González, M.; González-Calbet, J.; Dezanneau, G.; Estradé, S.; Peiró, F. Cation Disorder in $Sr_{0.67}Ba_{0.33}Nb_2O_6$ Assessed by Aberration Corrected STEM. *Results Mater.* **2019**, *3*, 100038.

(21) Olsen, G. H.; Selbach, S. M.; Grande, T. On the Energetics of Cation Ordering in Tungsten-Bronze-Type Oxides. *Phys. Chem. Chem. Phys.* **2015**, *17* (45), 30343−30351.

(22) Grendal, O. G.; Nylund, I.-E.; Blichfeld, A. B.; Tominaka, S.; Ohara, K.; Selbach, S. M.; Grande, T.; Einarsrud, M.-A. Controlled Growth of $Sr_xBa_{1-x}Nb_2O_6$ Hopper- and Cube-Shaped Nanostructures by Hydrothermal Synthesis. *Chem.—Eur J* **2020**, *26* (42), 9348−9355.

(23) Gardner, J.; Morrison, F. D. A-Site Size Effect in a Family of Unfilled Ferroelectric Tetragonal Tungsten Bronzes: $Ba_4R_{0.67}Nb_{10}O_{30}$ (R = La, Nd, Sm, Gd, Dy and Y). *Dalton Trans.* **2014**, *43* (30), 11687−11695.

(24) Kolodiaznyi, T.; Sakurai, H.; Isobe, M.; Matsushita, Y.; Forbes, S.; Mozharivskyj, Y.; Munsie, T. J. S.; Luke, G. M.; Gurak, M.; Clarke, D. R. Superconductivity and Crystal Structural Origins of the Metal-Insulator Transition in $Ba_{6-x}Sr_xNb_{10}O_{30}$ Tetragonal Tungsten Bronzes. *Phys. Rev. B* **2015**, *92* (21), 214508.
(25) O'Neill, H. S. C.; Navrotsky, A. Simple Spinels: Crystallographic Paramters, Cation Radii, Lattice Energies, and Cation Distribution. *Am. Mineral.* **1983**, *68*, 181−194.
(26) Hodeau, J.-L.; Favre-Nicolin, V.; Bos, S.; Renevier, H.; Lorenzo, E.; Berar, J.-F. Resonant Diffraction. *Chem. Rev.* **2001**, *101* (6), 1843−1868.
(27) Fernández-Carrión, A. J.; Ocaña, M.; Florian, P.; García-Sevillano, J.; Cantelar, E.; Fitch, A. N.; Suchomel, M. R.; Becerro, A. I. Crystal Structure and Luminescent Properties of Eu^{3+}-Doped A-$La_2Si_2O_7$ Tetragonal Phase Stabilized by Spray Pyrolysis Synthesis. *J. Phys. Chem. C* **2013**, *117* (40), 20876−20886.
(28) Fernández-Carrión, A. J.; Allix, M.; Ocaña, M.; García-Sevillano, J.; Cusso, F.; Fitch, A. N.; Suard, E.; Becerro, A. I. Crystal Structures and Photoluminescence across the $La_2Si_2O_7$-$Ho_2Si_2O_7$ System. *Inorg. Chem.* **2013**, *52* (23), 13469−13479.
(29) Fitch, A.; Dejoie, C.; Covacci, E.; Confalonieri, G.; Grendal, O.; Claustre, L.; Guillou, P.; Kieffer, J.; de Nolf, W.; Petitdemange, S.; Ruat, M.; Watier, Y. ID22, the High-Resolution Powder-Diffraction Beamline at ESRF. *J. Synchrotron Radiat.* **2023**, *30*, 1003−1012.
(30) Coelho, A. TOPAS and TOPAS-Academic: An Optimization Program Integrating Computer Algebra and Crystallographic Objects Written in C++. *J. Appl. Crystallogr.* **2018**, *51* (1), 210−218.
(31) Watts, B. Calculation of the Kramers-Kronig Transform of X-Ray Spectra by a Piecewise Laurent Polynomial Method. *Opt. Express* **2014**, *22* (19), 23628.
(32) Sasaki, S. Numerical Tables of Anomalous Scattering Factors Calculated by the Cromer and Liberman's Method. *KEK Report*, 1989; Vol. *88*(14), pp 1−136.
(33) Brown, I. D. 1 Historical Introduction. In *The Chemical Bond in Inorganic Chemistry*; Brown, I. D., Ed.; Oxford University Press, 2016, pp 1−8..
(34) Wills, A. S. VaList, Program Available at http://Fermat.Chem.Ucl.Ac.Uk/Spaces/Willsgroup/Software/Valist-Bond-Valence-Calculations-Listing/ (accessed March 20, 2023).
(35) Brown, I. D.; Altermatt, D. Bond-valence Parameters Obtained from a Systematic Analysis of the Inorganic Crystal Structure Database. *Acta Crystallogr., Sect. B: Struct. Sci., Cryst. Eng. Mater.* **1985**, *41* (4), 244−247.
(36) Jamieson, P. B.; Abrahams, S. C.; Bernstein, J. L. Ferroelectric Tungsten Bronze-Type Crystal Structures. II. Barium Sodium Niobate $Ba_{(4+x)}Na_{(2-2x)}Nb_{10}O_{30}$. *J. Chem. Phys.* **1969**, *50* (10), 4352−4363.
(37) Shannon, R. Revised Effective Ionic Radii and Systematic Studies of Interatomic Distances in Halides and Chalcogenides. *Acta Crystallogr., Sect. A* **1976**, *32* (5), 751−767.
(38) Whittle, T. A.; Howard, C. J.; Schmid, S. Structures and Phase Transitions in Barium Sodium Niobate Tungsten Bronze (BNN). *Acta Crystallogr., Sect. B: Struct. Sci., Cryst. Eng. Mater.* **2021**, *77* (6), 981−985.

https://doi.org/10.1021/acsomega.3c06500
ACS Omega 2023, 8, 37592−37599